Journal of ELECTRICAL ENGINEERING, VOL 71(2020), NO5, 340–346

sciendo

PAPERS

Performance analysis of optical fiber surface plasmon resonance sensor in single-mode operation region

Wael F. Abu Shehab

A new approach for studying the performance of single-mode optical fiber surface plasmon resonance sensor for refractive index sensing is presented. Intensity interrogation technique is used to observe and examine the effect of changing the value of the operating wavelength, within the single-mode operation region, on sensor performance. Effect of changing metal thickness, which is a critical parameter of the sensor structure, is also investigated. The results show that the selected operating wavelength within the mentioned region plays a very important role and has a significant impact on the sensor sensitivity. As the operating wavelength increases beyond the cut-off wavelength, above which the first higher-order mode disappears, the sensitivity increases while the refractive index range, for which the sensitivity is above its half maximum value, becomes narrower. In the proposed sensor structure, for a metal thickness of 25 nm, the maximum sensitivity reaches 2554 RIU^{-1} for analyte refractive index of 1.439 at a wavelength of 1500 nm. This sensitivity corresponds to a resolution of order 10^6 RIU by assuming 1% minimum reflectivity variation. The operating wavelength should be carefully selected and changed according to the refractive index values intended to be measured to ensure high sensor sensitivity at these values. The analysis provided in this paper enables to select and change the desired range of the sensed refractive index using low cost technique by just changing the operating wavelength in the single-mode operation region.

K e y w o r d s: surface plasmon resonance SPR, sensor, intensity interrogation, optical fiber, refractive index

1 Introduction

In recent years, optical fiber surface plasmon resonance (SPR) sensors have played an important role in medical, chemical, biological and environmental fields. Surface plasmons (SPs) are electron density oscillations that exist at the interface between two media having opposite signs of the real parts of their relative permittivities (such as metal-dielectric interface) and are considered as an electromagnetic wave that propagates along the interface. The field of SPs exponentially decays in the direction perpendicular to the interface (in the metal as well as the dielectric material). SPs can be optically excited using prism coupling, diffraction of light on a diffraction grating, and dielectric waveguides [1]. When an exciting light is coupled to the SPs under certain resonance condition, SPR occurs, which results in a dip in the light intensity.

In 1993, optical fiber has been used for the first time as a sensing element in SPR sensors to determine the changes in the sensed parameters [2]. Since that time, numerous designs have been proposed to improve the performance of the optical fiber SPR sensors. SPR sensors using various types of gratings such as fiber Bragg gratings [3], tilted fiber Bragg gratings [4], and long period gratings [5] have been presented. A tapered fiber structure based on localized SPR has been demonstrated in [6] for biomolecular sensing applications. The performance of these sensors has been also enhanced using different combinations of metals [7]. D-shaped polished fiber SPR sensors received a great deal of attention among researchers and have been proposed and studied in several researches such as in [8]. Besides the use of the metal thin film, sensors based on metallic nanowire have attracted significant attention and have been developed using localized SPR technology [9,10]. Several reviews concerning the optical fiber SPR sensors have been presented by researchers [11-15].

One of the major uses of optical fiber SPR sensors is measuring small refractive index changes of analytes. Wavelength (spectral) interrogation and intensity (amplitude) interrogation are the most commonly used techniques for these sensors. In the wavelength interrogation, changes of refractive index of the analyte are determined by monitoring the shift of the resonance wavelength, at which the dip of the reflected light intensity occurs [16,17]. In the intensity interrogation, the refractive index changes are determined by monitoring changes in the reflected light intensity at a fixed wavelength [16-18]. Each of these techniques has its advantages and disadvantages. The wavelength interrogation technique is accurate and immune to light source fluctuations. However, it has high cost due to its complexity and needing of expensive devices to perform spectral analysis. On the other hand, intensity interrogation technique does not require spectral analysis. However, it is not impervious to light intensity fluctuations.

To the best of our knowledge, no prior studies related to single-mode fiber SPR sensors (such as in [8] and [18-22]) have examined the effect of changing the value of the operating wavelength, while keeping the condition for single-mode operation, on the sensitivity of the SPR sensor.

Department of Electrical Engineering, Al-Hussein Bin Talal University, Maan 71111, Jordan, waelabushehab@ahu.edu.jo

DOI:10.2478/jee-2020–0046, Print (till 2015) ISSN 1335-3632, On-line ISSN 1339-309X

In order to achieve this, intensity interrogation technique is used in this paper, where sensitivities for some operating wavelengths, within the region that supports propagation of only the fundamental mode in the fiber, are determined. Linearly polarized (LP) modes are dealt with in this paper, since most fibers are weakly guiding due to their construction characteristics, where refractive index of the fiber core n_1 is approximately equal to refractive index of the cladding n_2 .

2 Sensor structure and principles

A four-layer D-type optical fiber SPR sensor shown in Fig. 1 is considered. In this sensor, a side-polished step-index optical fiber is used. The fiber cladding is partially removed and a metallic layer is applied on the polished side.

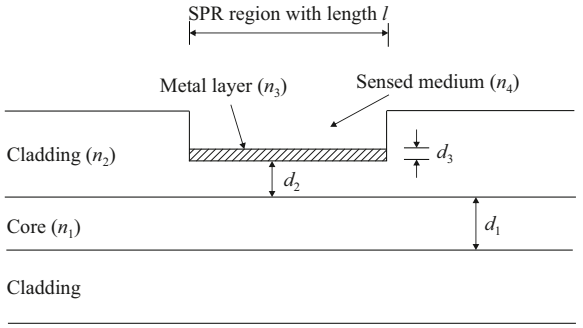

Fig. 1. The optical fiber SPR sensor

The length of the SPR region is l . The refractive indices of the core, the cladding, the metal, and the analyte (sensed medium) are n_1 , n_2 , n_3 , and n_4, respectively. The refractive indices of the core and cladding vary with the wavelength λ of the incident light (in micrometers) according to the Sellmeier equation [23]

$$n^2(\lambda) = 1 + \sum_{j=1}^{3} \frac{\lambda^2 A_j}{\lambda^2 - B_j^2}, \tag{1}$$

where A and B are Sellmeier coefficients. The relative permittivity and the refractive index of any metal can be determined using one of the dielectric function models, which can be found in many researches, such as Drude model, Lorentz-Drude model, and Brendel-Bormann model. Since the operating wavelengths used in this study are above 720 nm (to ensure single-mode operation of the fiber, as will be shown in section 3), Drude model has the best fit of the measured dielectric function in comparison with the other models [24]. Thus, it will be used to determine the relative permittivity and the refractive index of the metal as [25]

$$\epsilon_{r3} = 1 - \frac{\lambda^2 \lambda_c}{\lambda_p^2 (\lambda_c + j\lambda)}, \tag{2}$$

$$n_3 = \sqrt{\epsilon_{r3}}, \tag{3}$$

where λ_c and λ_p are the collision wavelength and the plasma wavelength of the metal, respectively.

The diameter of the core is d_1 and the thicknesses of the residual cladding and the metal are d_2 and d_3 , respectively. A light from monochromatic source is launched into one of the ends of the step-index fiber and propagates in the fiber core in the form of guided modes. Each of these modes has a distinct propagation constant. The number of the guided modes and their propagation constants are governed by the value of the normalized frequency or V parameter of the fiber, which is defined as [26]

$$V = \frac{2\pi}{\lambda} aNA\,, \tag{4}$$

where a is the core radius, and NA is the numerical aperture of the fiber.

For a particular wavelength, which is kept fixed in our case, the fiber supports certain number of guided modes. In this study, the fixed wavelength is chosen such that the value of the normalized frequency is less than 2.405. This condition guarantees single-mode operation of the fiber. The wavelength, above which the first higher-order mode disappears, is called cut-off wavelength, which can be simply found from equation (4). Thus, all operating wavelengths used in this study are chosen to be greater than the cut-off wavelength to ensure propagation of the fundamental mode only (LP_{01} as will be shown later). When this guided fundamental mode enter the SPR region, the evanescent field in the fiber transfers power to the SPs at the outer interface of the metal layer (metal-analyte interface). The coupling between the evanescent field and the SPs depends strongly on the refractive index of the analyte. Therefore, very small changes in this index produce coupling strength changes, which cause changes in the reflected light intensity detected at the other end of the fiber. At a certain value of the refractive index of the analyte, maximum power is transferred to the SPs, which causes a dip in the reflected light intensity. The propagation constant of the fundamental mode can be determined by solving the characteristic equation (or dispersion relation) for LP modes [26]

$$u\frac{J_1(u)}{J_0(u)} = w\frac{K_1(w)}{K_0(w)}, \tag{5}$$

where J_0 and J_1 are the Bessel functions of the first kind and of order 0 and 1, respectively. K_0 and K_1 are the modified Bessel functions of the second kind and of order 0 and 1, respectively. u and w are the normalized transverse propagation constants for which it holds that [26]

$$u^2 + w^2 = V^2, \tag{6}$$

$$u = ak_T, \tag{7}$$

where k_T is the transverse propagation constant, that is defined as [26]

$$k_T^2 = (\frac{2\pi}{\lambda} n_1)^2 - \beta^2, \tag{8}$$

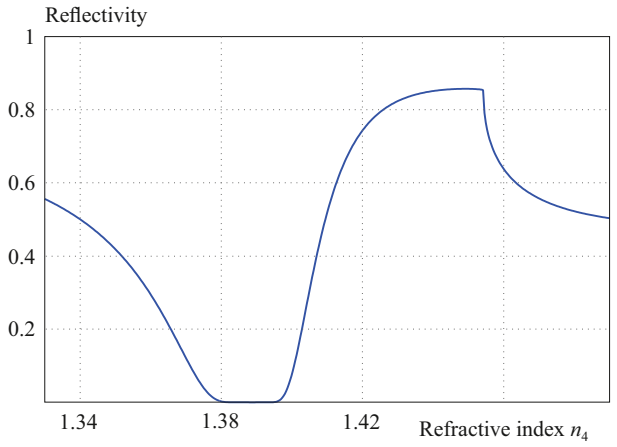

Fig. 2. Reflectivity versus refractive index n_4 at $\lambda = 720$ nm

β is the longitudinal propagation constant (hereinafter referred to as the propagation constant), which can be written in terms of angle θ (with respect to the normal to the core-cladding interface) of the incident light by [26]

$$\beta = \frac{2\pi}{\lambda} n_1 \sin\theta. \tag{9}$$

The propagation constant of the fundamental mode is denoted as β_{01} and the mode itself is denoted as LP_{01} . β_{01} can have different values according to the operating wavelength. To study the effect of changing the value of the operating wavelength, within the single mode operation region, on the sensor sensitivity, the reflectivity of the fundamental mode should be determined. The reflection coefficient of the four-layer structure shown in Fig. 1 can be written as [18,21]

$$r_{1234} = \frac{r_{12} + r_{234} e^{j2k_2 d_2}}{1 + r_{12} r_{234} e^{j2k_2 d_2}}, \tag{10}$$

where

$$r_{234} = \frac{r_{23} + r_{34} e^{j2k_3 d_3}}{1 + r_{23} r_{34} e^{j2k_3 d_3}}, \tag{11}$$

$$r_i j = \frac{k_i/n_i^2 - k_j/n_j^2}{k_i/n_i^2 + k_j/n_j^2}, \quad \text{for } i = 1,2,3 \text{ and } j = i+1, \tag{12}$$

$$k_{i(\text{or}j)} = \frac{2\pi}{\lambda} \sqrt{n_{i(\text{or}j)}^2 - n_1^2 \sin^2\theta)}. \tag{13}$$

The power reflection coefficient or reflectivity R' of the structure for a single reflection is then [18,21]

$$R' = |r_{1234}|^2. \tag{14}$$

If the number of reflections within the sensor of length l is m , the total reflectivity R can be expressed as [18,21]

$$R = R'^m, \tag{15}$$

where

$$m = \frac{l}{4a \tan\theta}. \tag{16}$$

The sensor sensitivity for intensity interrogation technique can be determined by [18]

$$S = \left| \frac{\partial R}{\partial n_4} \right|. \tag{17}$$

Finally, the resolution of the sensor can be defined as the smallest change in analyte refractive index detectable in the sensor output. It depends on the sensor properties as well as the accuracy of the monitoring device [27]. In this paper, it is calculated by assuming a minimum reflectivity variation of 1% [28].

3 Results and discussion

The parameters of the sensor that are used in the simulation are: fiber core diameter $d_1 = 7$ μm, residual cladding thickness $d_2 = 10$ nm , metal thickness $d_3 = 35$ nm, and sensing length $l = 4$ mm. The fiber core and cladding are assumed to be made of undoped silica and fluorine-doped silica, respectively. The Sellmeier coefficients A and B, used to determine the refractive indices have the following values, [23]

for core		for cladding	
(-)	(μm)	(-)	(μm)
$A_1 = 0.6969$	$B_1 = 0.0691$	$A_1 = 0.6919$	$B_1 = 0.0684$
$A_2 = 0.4082$	$B_2 = 0.1157$	$A_2 = 0.4079$	$B_2 = 0.1162$
$A_3 = 0.8908$	$B_3 = 9.9010$	$A_3 = 0.8975$	$B_3 = 9.8960$

Gold metal (Au) is used in the simulation due to its chemical stability. λ_c and λ_p for gold are 8.9342×10^{-6} m and 1.6826×10^{-7} m, respectively [25]. Table 1 shows refractive index of the gold for some operating wavelengths used in the study.

Table 1. Refractive index of the gold for some operating wavelengths

Wavelength (nm)	Refractive index
720	0.1766+j4.1501
1000	0.3348+j5.8307
1200	0.4784+j7.0136
1500	0.7402+j8.7660

The fixed wavelength is chosen such that to ensure the condition of single-mode operation. Thus, the fundamental LP_{01} mode is only guided in the fiber and all other modes are cut off.

All calculations in the study are performed by inserting all equations presented in section 2, in addition to the above mentioned parameters, into MATLAB platform-version R2013a.

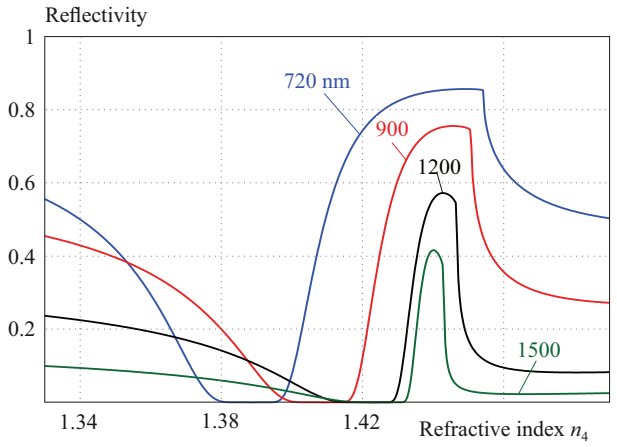

Fig. 3. Reflectivity versus refractive index n_4 for different wavelengths

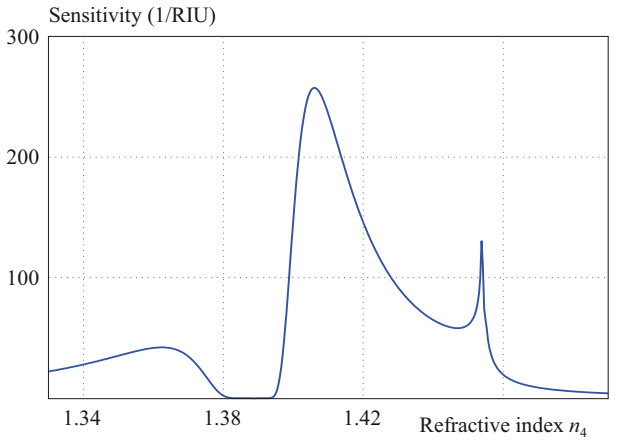

Fig. 4. Sensitivity versus refractive index n_4 at $\lambda = 720$ nm

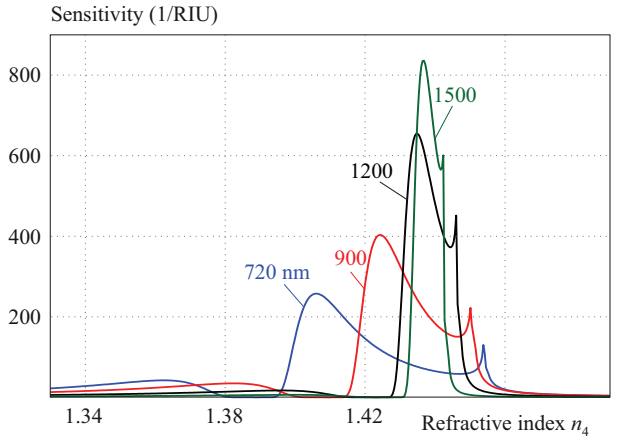

Fig. 5. Sensitivity versus refractive index n_4 for different wavelengths

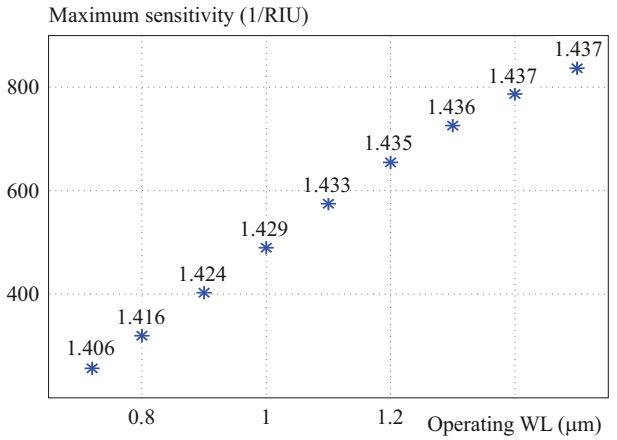

Fig. 6. Maximum sensitivities reached at certain values of n_4 (written above the data points) for different operating wavelengths

Figure 2 shows the reflectivity versus the analyte refractive index n_4 when the wavelength is at $\lambda = 720$ nm. At this wavelength (which is greater than the cut-off wavelength of 715.7 nm), the normalized frequency is equal to 2.3914, which allows only the fundamental mode to be propagated with a normalized transverse propagation constant u that is approximately equal to 1.64314. It can be noted that the dip in the reflectivity (which indicates the maximum coupling between the fundamental mode and the SPs) occurs when $n_4 = 1.389$.

Figure 3 shows the reflectivity versus n_4 for the wavelengths 720, 900, 1200, and 1500 nm. At all of these wavelengths, the LP_{01} mode is the only mode that is propagated in the fiber. It is clear from this figure that the value of n_4 at the dip increases with operating wavelength increasing. For example, at $\lambda = 1200$ nm, $n_4 = 1.423$ at the dip.

The sensitivity of the sensor as a function of n_4 at $\lambda = 720$ nm is shown in Fig. 4. At this operating wavelength, the maximum sensitivity is 257 RIU $^{-1}$ (1/refractive index unit) which can be reached for $n_4 = 1.406$. This value of sensitivity corresponds to a resolution of 3.891×10^{-5} RIU by assuming 1% minimum reflectivity variation.

The dependence of the sensitivity on n_4 for different wavelengths is shown in Fig. 5. It can be deduced that the maximum sensitivity increases by increasing the operating wavelength (away from the cut-off wavelength). For example, the sensitivity reaches 837 RIU $^{-1}$ for $n_4 = 1.437$ at $\lambda = 1500$ nm (the corresponding resolution is 1.195×10^{-5} RIU). However, the analyte refractive index range, for which the sensitivity is above its half maximum value, becomes narrower by increasing the operating wavelength. This also holds for wavelengths beyond 1500 nm. It is good to mention here that having a wide range of the measured refractive indices for a certain operating wavelength is important and desirable from the practical point of view.

Figure 6 shows the maximum sensitivities for some operating wavelengths. The values of n_4, at which the maximum sensitivities are reached, are written above the data points in this figure. Thus, according to the approximate n_4 values intended to be measured, an appropriate operating wavelength should be selected and used to ensure high sensor sensitivity at these values.

One of the most important and critical parameters of sensor structure that must be considered when studying sensor performance is metal thickness d_3. Figure 7 shows

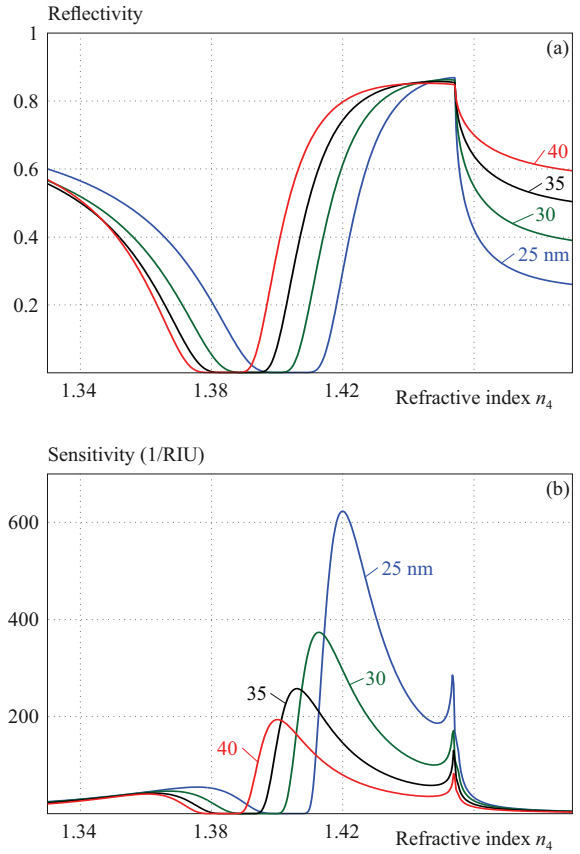

Fig. 7. (a) – reflectivity, and (b) – sensitivity *vs* n_4 for different metal thicknesses d_3 at $\lambda = 720$ nm

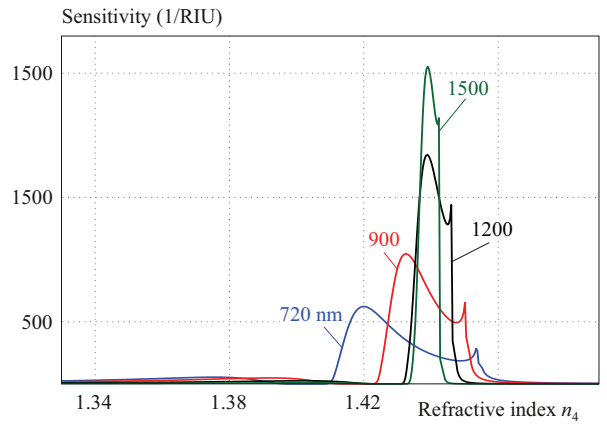

Fig. 8. Sensitivity *vs* refractive index n_4 for different wavelengths when $d_3 = 25$ nm

the reflectivity and the sensitivity versus refractive index n_4 for different metal thicknesses d_3 at $\lambda = 720$ nm. It is obvious from Fig. 7(a) that if d_3 is decreased, the value of n_4 at the dip increases. For example, when $d_3 = 40$ nm, the value of n_4 at the dip is 1.384. If d_3 decreases to 25 nm, n_4 increases to 1.404. Also, it is obvious from Fig. 7(b) that the maximum sensitivity can be increased to higher values by decreasing d_3. For example, the maximum sensitivity is near 194 RIU $^{-1}$ when $d_3 = 40$ nm for $n_4 = 1.400$ (the corresponding resolution is 5.155×10^{-5} RIU) and it reaches 623 RIU $^{-1}$ when d_3 is decreased to 25 nm for n_4 =1.420 (the corresponding resolution is 1.605×10^{-5} RIU). Thus, by decreasing d_3, maximum sensitivity increases and reaches high values within some locations of n_4, which are also shifted to higher values.

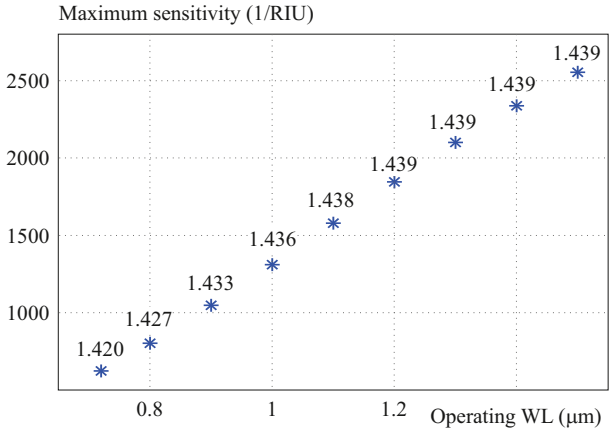

Fig. 9. Maximum sensitivities reached at certain values of n_4 (written above the data points) for different operating wavelengths when $d_3 = 25$ nm.

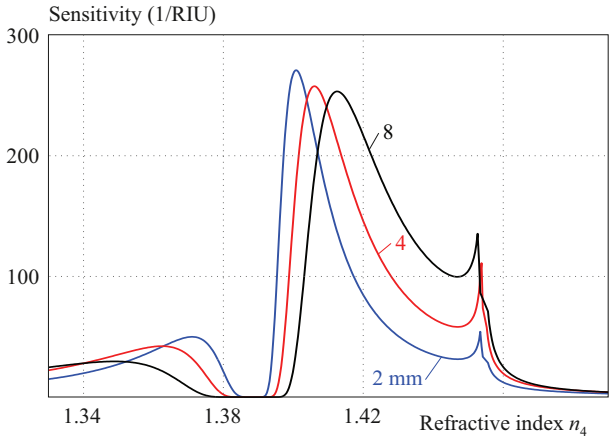

Fig. 10. Sensitivity *vs* refractive index n_4 for different sensor lengths l at $\lambda = 720$ nm and $d_3 = 35$ nm

Figure 8 shows the sensitivity versus refractive index n_4 for different wavelengths when $d_3 = 25$ nm. The maximum sensitivity increases by increasing the operating wavelength. It reaches 2554 RIU $^{-1}$ at $\lambda = 1500$ nm for $n_4 = 1.439$ (the corresponding resolution is 3.915×10^{-6} RIU). The effect of decreasing metal thickness from 35 nm to 25 nm on the sensitivity is evident when comparison is made between Fig. 8 and Fig. 5.

Figure 9 shows the maximum sensitivities for some operating wavelengths when $d_3 = 25$ nm. The values of n_4, at which the maximum sensitivities are reached, are written above the data points.

The effect of changing sensor length l is considered and shown in Fig. 10, which illustrates the sensitivity for different lengths l at $\lambda = 720$ nm and $d_3 = 35$ nm. It can be noted that the increasing of sensor length causes a shift of maximum sensitivity toward higher values of n_4.

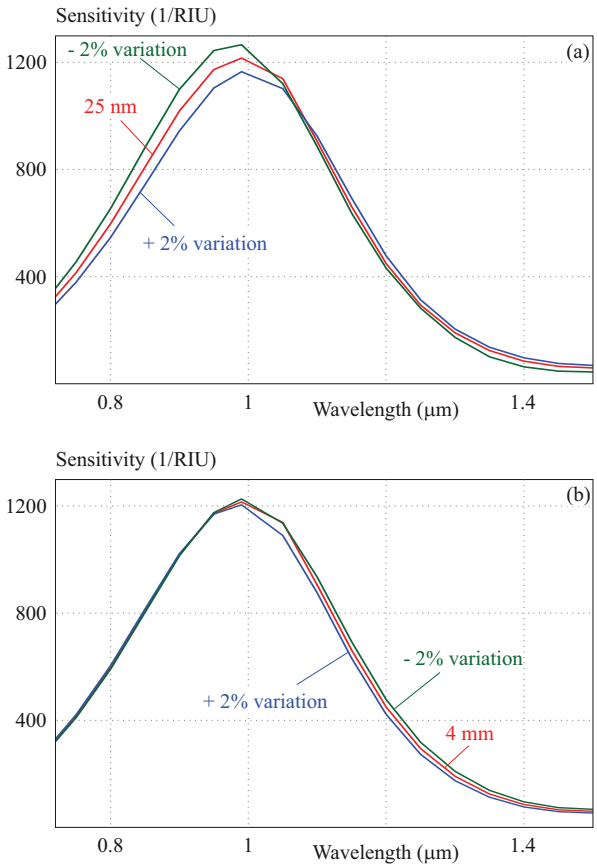

Fig. 11. Sensitivity *vs* wavelength for $n_4 = 1.434$: (a) – with 2% variation of the metal thickness ($d_3 = 25$ nm), and (b) – with 2% variation of the sensor length ($l = 4$ mm)

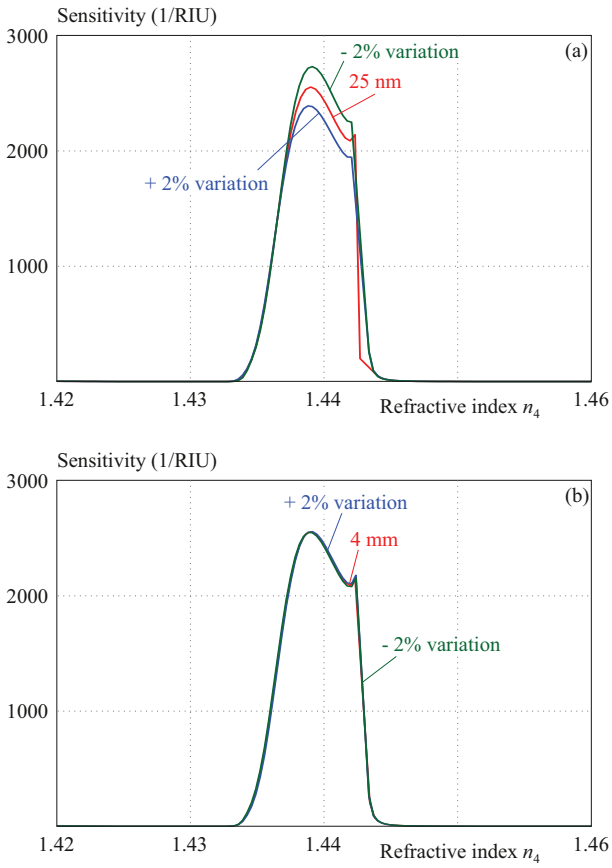

Fig. 12. Sensitivity *vs* analyte refractive index for $\lambda = 1500$ nm: (a) – with 2% variation of the metal thickness ($d_3 = 25$ nm) and (b) with 2% variation of the sensor length ($l = 4$ mm)

Table 2. Performance comparison of some reported SPR sensors

Ref.	Structure type	Sensitivity (RIU^{-1})	Resolution (RIU)
[6]	Single mode tapered fiber	-	32×10^{-6}
[16]	Photonic crystal fiber	2843	3.5×10^{-6}
[17]	D-shaped photonic crystal fiber	1054	16.7×10^{-6}
[18]	D-type single mode fiber	40	25×10^{-6}
[29]	Bimetal coated fiber	-	5.8×10^{-6}
This work	D-type single mode fiber	2554	3.915×10^{-6}

Finally, it is important to show the fabrication tolerance of the sensor, since a small variation of 1% may take place during the fabrication process [9]. The effect of the metal thickness and the sensor length with 2% fabrication tolerance on the sensor performance is shown in Fig. 11, where the sensitivity versus the wavelength for $n_4 = 1.434$ with 2% variation of the metal thickness ($d_3 = 25$ nm) and 2% variation of the sensor length ($l = 4$ mm) are illustrated in Fig. 11(a) and Fig. 11(b).

In addition, Fig. 12(a) and Fig. 12(b) show the sensitivity versus the analyte refractive index at $\lambda = 1500$ nm with 2% variation of the metal thickness and the sensor length, respectively. From these figures, it can be deduced that the sensor can perform effectively with the 2% variation of the metal thickness and the sensor length.

A performance comparison of some reported SPR sensors that use intensity interrogation is shown in Tab. 2.

4 Conclusion

Intensity interrogation technique is used to investigate the performance of optical fiber SPR sensor when the fiber supports only propagation of the fundamental mode. The chosen value of the operating wavelength, for which the normalized frequency is less than 2.405, affects significantly on the sensor sensitivity. According to the n_4 values intended to be measured, an appropriate operating wavelength should be selected and used to ensure high sensor sensitivity at these values. In the wavelength

region between 720 nm and 1500 nm and for the metal thickness $d_3 = 35$ nm, the results show that as the wavelength increases, the maximum sensitivity increases and reaches 837 RIU^{-1} for $n_4 = 1.437$ at $\lambda = 1500$ nm (the corresponding resolution is 1.195×10^{-5} RIU by assuming 1% minimum reflectivity variation). However, the analyte refractive index range, for which the sensitivity is above its half maximum value, becomes narrower by increasing the operating wavelength. If d_3 decreases to 25 nm, then as the wavelength increases, the maximum sensitivity increases and reaches 2554 RIU $^{-1}$ for $n_4 = 1.439$ at $\lambda = 1500$ nm (the corresponding resolution is 3.915×10^{-6} RIU). It has also been shown that the sensor can perform effectively with 2% variation of the metal thickness and the sensor length. The range of the analyte refractive index, for which the sensor has high sensitivity, can be changed to desired values by changing the parameters of the sensor structure and by following the procedures described in this paper.

References

[1] J. Homola, " Electromagnetic theory of surface plasmons", *Surface plasmon resonance based sensors, Springer Series on Chemical Sensors and Biosensors*, (J. Homola, ed.), Springer, Berlin, Heidelberg, 2006, DOI: 10. 1007/5346_013.

[2] R. C. Jorgenson and S. S. Yee, "A Fiber-Optic Chemical Sensor Based on Surface Plasmon Resonance", *Sensors and Actuators B-Chemical*, vol. 12, no. 3, pp. 213-220, 1993.

[3] P. Arasu, A. S. M. Noor, A. Shabaneh, M. H. Yaacob, H. N. Lim, and M. Mahdi, "Fiber Bragg Grating Assisted Surface Plasmon Resonance Sensor with Graphene Oxide Sensing Layer", *Optics Communications*, vol. 380, pp. 260-266, 2016.

[4] M. Lobry, K. Chah, M. Loyez, D. Kinet, and C. Caucheteur, "Refractometric Sensing with Plasmonic Tilted Bragg Gratings Different Fiber Types", *Proc. SPIE 11354, Optical Sensing and Detection VI, 113542W*, (1 April 2020), 2020.

[5] W. Wei, J. Nong, G. Zhang, L. Tang, X. Jiang, N. Chen, S. Luo, G. Lan, and Y. Zhu, "Graphene-Based Long-Period Fiber Grating Surface Plasmon Resonance Sensor for High-Sensitivity Gas Sensing", *Sensors*, vol. 17, no. 1, 2017.

[6] L. Hsing-Ying, H. Chen-Han, C. Gia-Ling. , C. Nan-Kuang, and C. Hsiang-Chen, "Tapered Optical Fiber Sensor Based on Localized Surface Plasmon Resonance", *Optics Express*, vol. 20, no. 19, pp. 21693-21701, 2012.

[7] R. Tabassum and B. D. Gupta, "SPR Based Fiber-Optic Sensor with Enhanced Electric Field Intensity and Figure of Merit using Different Single and Bimetallic Configurations", *Optics Communications*, vol. 367, pp. 23-34, 2016.

[8] N. A. M. Zainuddin, M. M. Ariannejad, P. T. Arasu, S. W. Harun, and R. Zakaria, "Investigation of Cladding Thicknesses on Silver SPR Based Side-Polished Optical Fiber Refractive-Index Sensor", *Results Physics*, vol. 13, 102255, 2019.

[9] A. K. Pathak, B. M. A. Rahman, V. K. Singh, and S. Kumari, "Sensitivity Enhancement of a Concave Shaped Optical Fiber Refractive Index Sensor Covered with Multiple Au Nanowires", *Sensors*, vol. 19, no. 19, 4210, 2019.

[10] A. K. Pathak and V. K. Singh, "SPR Based Optical Fiber Refractive Index Sensor Using Silver Nanowire Assisted CSMFC", *IEEE Photonics Technology Letters*, vol. 32, no. 8, pp. 465-468, 2020.

[11] A. K. Sharma, R. Jha, and B. D. Gupta, "Fiber-Optic Sensors Based on Surface Plasmon Resonance: A Comprehensive Review", *IEEE Sensors Journal*, vol. 7, no. 8, pp. 1118-1129, 2007.

[12] M. S. A. Gandhi, S. Chu, K. Senthilnathan, P. R. Babu, K. Nakkeeran, and Q. Li, "Recent Advances Plasmonic Sensor-Based Fiber Optic Probes for Biological Applications", *Applied Sciences*, vol. 9, no. 5, 2019.

[13] B. A. Prabowo, A. Purwidyantri, and K. Liu, "Surface Plasmon Resonance Optical Sensor: A Review on Light Source Technology", *Biosensors*, vol. 8, no. 3, 80, 2018.

[14] E. Klantsataya, P. Jia, H. Ebendorff-Heidepriem, T. M. Monro, and A. Francois, "Plasmonic Fiber Optic Refractometric Sensors: from Conventional Architectures to Recent Design Trends", *Sensors*, vol. 17, no. 1:12, 2017.

[15] Y. E. Monfared, "O", *rview of Recent Advances the Design of Plasmonic Fiber-Optic Biosensors*, Biosensors, vol. 10, no. 7, 77, 2020.

[16] F. Haider, R. A. Aoni, R. Ahmed, and A. E. Miroshnichenko, "Highly Amplitude-Sensitive Photonic Crystal Fiber Based Plasmonic Sensor", *Journal of the Optical Society of America B*, vol. 35, no. 11, pp. 2816-2821, 2018.

[17] E. Haque, Md. A. Hossain, F. Ahmed, and Y. Namihira, "Surface Plasmon Resonance Sensor Based on Modified D-Shaped Photonic Crystal Fiber for Wider Range of Refractive Index Detection", *IEEE Sensors Journal*, vol. 18, no. 20, pp. 8287-8293, 2018.

[18] M. H. Chiu, C. H. Shih, and M. H. Chi, "Optimum Sensitivity of Single-Mode D-Type Optical Fiber Sensor the Intensity Measurement", *Sensors and Actuators B-chemical*, vol. 123, no. 2, pp. 11201124, 2007.

[19] A. V. Dyshlyuk, O. B. Vitrik, and Y. N. Kulchin, "Application of Optical Fibres with Reduced Normalized Frequency for SPR-Based Refractometry", *Pacific Science Review A: Natural Science and Engineering*, vol. 17, pp. 35-37, 2015.

[20] M. H. Chiu and C. H. Shih, "Searching for Optimal Sensitivity of Single-Mode D-type Optical Fiber Sensor the Phase Measurement", *Sensors and Actuators B-chemical*, vol. 131, no. 2, pp. 596601, 2008.

[21] M. F. Ubeid and M. M. Shabat, "Analytical Sensitivity and Reflected Power through a D-Shape Optical Fibre Sensor", *OptoElectronics Review*, vol. 22, no. 3, pp. 191195, 2014.

[22] A. K. Pathak, V. K. Singh, S. Ghosh, and B. M. A. Rahman, "Investigation of a SPR Based Refractive Index Sensor using a Single Mode Fiber with a Large D Shaped Microfluidic Channel", *OSA Continuum*, vol. 2, no. 11, pp. 3008-3018, 2019.

[23] A. Mendez and T. F. Morse, *Specialty optical fibers handbook* San Diego, California, USA Academic Press, pp. 1968, 2007.

[24] A. R. Sarhan, B. B. Yousif, N. F. F. Areed, and S. S. A. Obaya, "Modeling of Fiber Optic Gold SPR Sensor using Different Dielectric Function Models: A Comparative Study", *Plasmonics*, 2020.

[25] S. Singh, R. S. Kaler, and S. Sharma, "A Novel Two-Dimensional Material Based Optical Fiber Surface Plasmon Resonance Sensor for Sensing of Organic Compounds Infrared Spectrum Window", *Journal of Communications Technology and Electronics*, vol. 68, no. 11, pp. 1269-1275, 2018.

[26] B. E. A. Saleh and M. C. Teich, *Fundamentals of photonics*, 3rd edition, Hoboken, NJ, USA, John Wiley & Sons, 2019.

[27] R. Kashyap and G. Nemova, "Surface Plasmon Resonance-Based Fiber and Planar Waveguide Sensors", *Journal of Sensors*, vol. 2009, pp. 1-9, 2009.

[28] A. A. Rifat, G. A. Mahdiraji, Y. M. Sua, Y. G. Shee, R. Ahmed, D. M. Chow, and F. R. M. Adikan, "Surface Plasmon Resonance Photonic Crystal Fiber Biosensor: A Practical Sensing Approach", *IEEE Photonics Technology Letters*, vol. 27, no. 15, pp. 1628-1631, 2015.

[29] T. T. Nguyen, L. Eun-Cheol, and J. Heongkyu, "Bimetal Coated Optical Fiber Sensors Based on Surface Plasmon Resonance Induced Change Birefringence and Intensity", *Optics Express*, vol. 22, no. 5, pp. 5590-5598, 2014.

Received 8 July 2020